Journal of Contaminant Hydrology 243 (2021) 103911

Contents lists available at ScienceDirect

Journal of Contaminant Hydrology

journal homepage: www.elsevier.com/locate/jconhyd

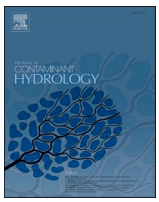

Temporal-Spatial changes of monthly vegetation growth and their driving forces in the ancient Yellow river irrigation system, China

Kailong Li [a], Guohe Huang [a,*], Xiaoyue Zhang [a], Chen Lu [a], Shuo Wang [b]

[a] Faculty of Engineering, University of Regina, Regina, Saskatchewan S4S 0A2, Canada
[b] Department of Land Surveying and Geo-Informatics, Hong Kong Polytechnic University, Hong Kong, China

ARTICLE INFO

Keywords:
Leaf area index
Mann Kendall trend analysis
Stepwise clustered analysis
Reginal climate model projection

ABSTRACT

Irrigation systems play vital roles not only in food production but also in supporting ecosystems. Understanding how the ecosystem has evolved in response to human activities is crucial for sustainable food production, especially for arid and semi-arid regions. In this study, we examined the trends of vegetation growth on a monthly basis in the ancient Yellow River irrigation system in Ningxia, China. We used the leaf area index (LAI) to characterize the vegetation growth from 2007 to 2019. The LAI trends were associated with a series of driving forces, explaining the spatial and temporal change of vegetation growth. With the provision of the Wilks feature importance method, 2-month averaged air temperature and irrigation were identified as the two most important variables for monthly LAI simulation. Future climate projections based on the Regional Climate Model system (RegCM) suggested dryer and longer summers under the RCP 8.5 scenario. These changes will increase the crop water demand during the growing months. In the future, water conflict might be further intensified in May, in which the present irrigation water has already led to a decreased crop growth. Our findings demonstrated that the Mann Kendall monthly trend analysis could provide more helpful information for monitoring the vegetation growth than the trend analysis on a yearly and seasonal basis.

1. Introduction

Traditional irrigation systems have evolved from the simple function of delivering water resources for food production (Raheem et al., 2015). These systems now also play vital roles in providing ecological services, especially in arid and semi-arid regions where nature restoration alone cannot amend the degrading ecosystems owing to intensive human activities. Therefore, understanding the underlying mechanisms for ecosystem evolutions is critical in improving the capacities of irrigation systems. However, due to the complexity of irrigation systems and the uncertainty of climate change, current understandings for ecosystem evolutions in irrigation systems are still limited (Gregory et al., 2018; Liu et al., 2009; Mu, 2000). Consequently, it is much desired to precisely describe the changes of ecosystems temporally and spatially and identify the key influencing factors in response to these changes.

Leaf Area Index (LAI) is one of the essential biophysical variables for characterizing land surface ecosystems (Jiang et al., 2010). It is defined as the one-sided green leaf area per unit ground area. In needle leaf vegetation, LAI is defined as the projected needle leaf area per unit ground area (Buermann et al., 2002). LAI is closely linked to many key ecological processes such as photosynthesis, transpiration, carbon and nutrient cycle, as well as evapotranspiration. Thus LAI is widely used to estimate net primary productivity and other quantities (Chen and Cihlar, 1996; Jiang et al., 2010). From the perspective of earth sciences, LAI affects the exchange of substance, energy, and momentum between the land surface and atmosphere (Monteith and Unsworth, 2013) and serves as critical input or key variable in most simulation models of climate, hydrology, and biogeochemistry (Karimi, 2020; Yin, 2017). The two predominant approaches to obtain the LAI are ground-based and remote sensing (*RS*)-based approaches (Breda, 2003). Even though the ground-based method for measuring LAI is more accurate than the RS-based one, it only suitable for a small scale (Yin et al., 2017). For most earth science related studies, RS-based LAI products are much preferred for their availability for long-term, large scale and continuous observations.

RS-based LAI products are routinely produced from various satellite data such as MODIS (Moderate Resolution Imaging Spectroradiometer), SPOT-VEGETATION, Multiangle Imaging SpectroRadiometer (MISR), and so on (Jiang et al., 2010; Xiao et al., 2017). These LAI time series products have been used to examine the dynamic changes of vegetation

* Corresponding author at: 3737 Wascana Pkwy, Regina, Saskatchewan, Canada.
E-mail address: huangg@uregina.ca (G. Huang).

https://doi.org/10.1016/j.jconhyd.2021.103911
Received 6 February 2021; Received in revised form 29 August 2021; Accepted 17 October 2021
Available online 20 October 2021

cover and associated ecosystems. From a global perspective, Alton (2018) examined the decadal trends (through linear regression) in photosynthetic capacity and LAI to ascertain the biochemical and structural responses of vegetation to environmental change. They found that the decadal trends were of a sufficient magnitude to influence vegetation productivity and carbon uptake. Zhu et al. (2017) investigated the seasonal mean LAI trends at northern latitudes (north of 30°N) between 1982 and 2009 using three RS-based LAI products. They found that climate change controls the spatial pattern of seasonal LAI trends and dominates the increase in seasonal LAI in the northern high-latitudes. Jiang et al. (2017) compared four long-term global LAI products in terms of trends, interannual variabilities, and uncertainty variations from 1982 through 2011. Rasul et al. (2020) examined the trend and linear regression modeling of LAI derived from the MODIS data. In their study, the relationships between LAI and LST were assessed across the continents. More recently, Cortés et al. (2021) employed the Mann Kendall test (Kendall, 1948; Mann, 1945) to detect the annual trend of LAI globally with the time span of 2000–2018. They reported evidence for an increasing seasonal amplitude in LAI north of 35°N.

From a regional perspective, Yin et al. (2017) used the ensemble empirical mode decomposition (EEMD) method and the GIMMS LAI dataset from 1982 to 2010 to analyze the nonlinear feature and spatial difference of forest LAI over China for the past 29 years. Their results indicated that the national-averaged forest LAI was characterized by quasi-3- and quasi-7-year oscillations, which generally exhibited a rising trend with an increasing rate. Liang et al. (2015) investigated the spatial-temporal characteristics and interrelationships of the vegetation dynamics and climate variability in Xinjiang Province, China, using the GLASS LAI dataset and a gridded meteorological dataset from 1982–2012. Their results suggested a significant increasing trend of vegetation growth in the oases and a significant decreasing trend of vegetation growth in certain areas. Reygadas et al. (2019) detected forest degradation by analyzing the trend component of the time series of LAI collected by the MODIS over Central Mexico from 2002 to 2017. More recently, Zhang et al. (2021) explored vegetation stability, tendency, and sustainability in the Three-River Source Region, China, with multiple methods based on the 2000–2017 GLASS LAI product. In their results, differentiation patterns of LAI variations and multiyear mean LAI value under different topographic factors were investigated.

Even though the studies mentioned above have provided concrete frameworks for detecting LAI trends and the associated driving forces, most of these assessment efforts focused on interannual LAI trends (Reygadas et al., 2019; Yuan, 2021; Zhang, 2021). Only one of these studies focused on the seasonal averaged LAI trends (Zhu et al., 2017). There has been no attempt to evaluate the trends of monthly averaged LAI. In fact, assessing the trends of monthly averaged LAI is critical for understanding the relationships between the land surface and atmosphere at a finer temporal resolution. It is acknowledged that climate change not only influences the annual mean values of climate variables but also influences the interannual climate variability (Shrestha and Wang, 2020; Wang et al., 2006). The frequencies and extremes of climatic indices may impose a much larger impact on vegetation growth than the annual mean values do (Alton, 2018). In irrigated watersheds, understanding the interannual climate variability on a monthly basis is more important than pristine watersheds because one wants to know the exact time to begin planting. Relating trends of monthly averaged LAI with the associated driving forces can improve our understanding of its underlying mechanism.

Therefore, the objective of this study is to investigate the trends of monthly averaged LAI in an irrigated watershed and explore its potential driving forces in terms of qualitative and quantitative manners. The objective entails (1) detecting the trend of monthly MODIS LAI time series in the ancient Yellow River irrigation system, China, from 2007 to 2019; (2) investigating the potential driving forces of the monthly LAI change through correlation analysis to understand the temporal and spatial changes of vegetation growth; (3) modeling monthly LAI with the Stepwise Clustered Ensemble (SCE) to identify the relative importance of several contributing variables; and (4) inferring the future changes for the vegetation growth based on the climate projections from Regional Climate Model (RegCM).

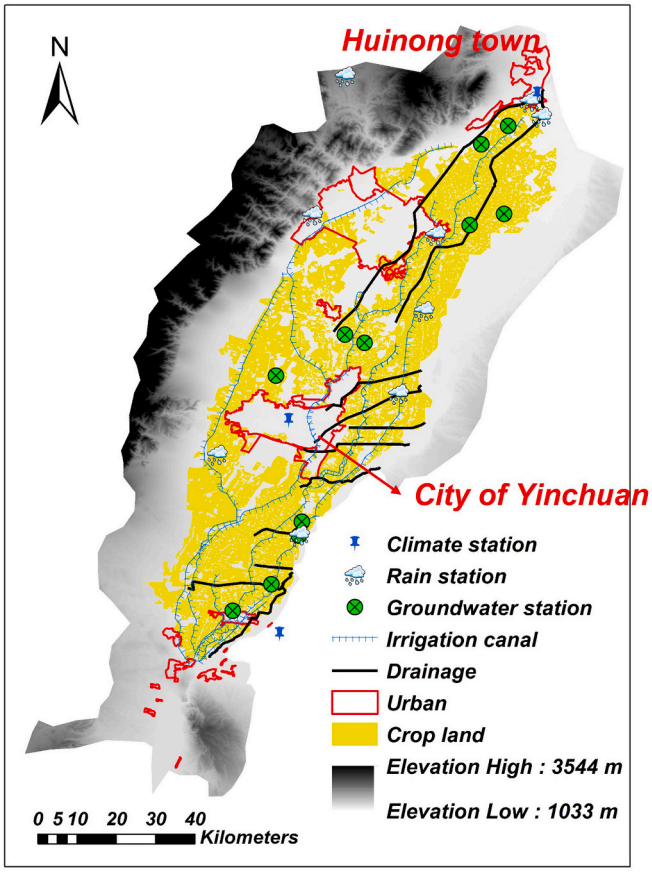

Fig. 1. Map of the study area.

2. The ancient Yellow River irrigation system

The ancient Yellow River irrigation system (AYRIS) in Ningxia is the oldest Yellow River irrigation system in North China, with a total area of 660,000 ha and an irrigated area of 552,000 ha. The AYRIS has been well documented since 215 BCE in the Qin dynasty (Zhang and Deng, 1987) when the first settlers opened canals from the Yellow River and started irrigation. During the successive 2000 years, the irrigation systems had been advanced significantly. From 1722 to 1735 in the Qing dynasty, it became a sophisticated irrigation system serving an irrigation area of 146,700 ha (Lu, 2019). The construction of Qingtongxia dam in 1959 tremendously advanced the irrigation system by elevating the water head, and the irrigation area was increased to 330,000 ha. The AYRIS has been recognized as a world irrigation heritage in 2017 (International Commission on Irrigation and Drainage).

As the West part of the AYRIS, the study area is located at the West alluvial plain of the Yellow River, crisscrossed by six main irrigation canals and numerous drainages. Fig. 1 shows the detailed layout of the AYRIS. This area is endowed for the abundant heat (i.e., 10C° above the accumulative temperature ranges from 3200C° to 3400C°) during the farming season (i.e., April to September), the adequate radiation (i.e., 148 cal/cm^2·a) and the long non-frost days (i.e., 164 days in average). These natural advantages combined with the sediment-rich irrigation water have benefited various crops through flood irrigation.

The study area is characterized by an arid climate with the high potential evaporation ranging from 1100 to 1600 mm (gauged by E601)

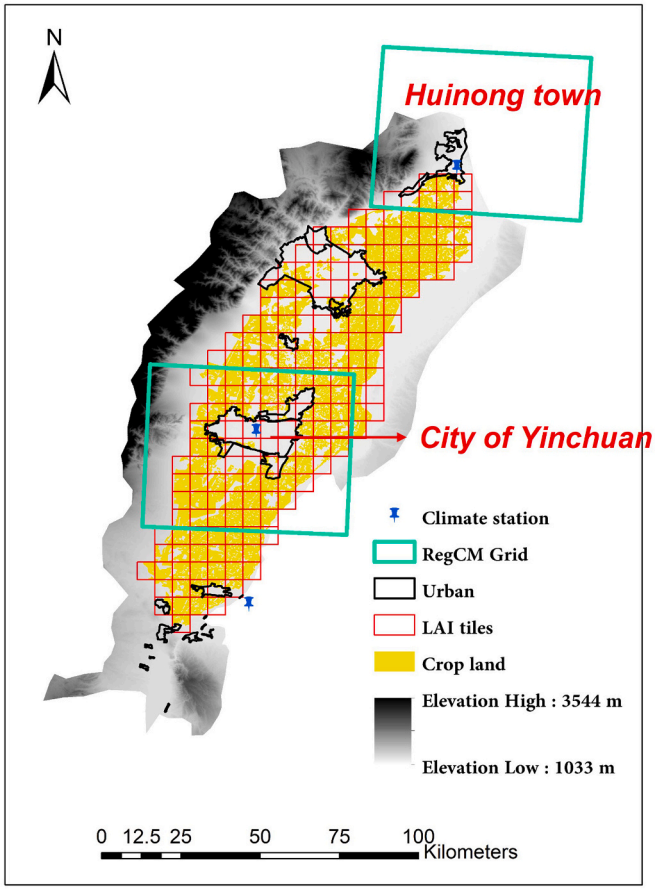

Fig. 2. LAI tiles and RegCM grids in the study area.

and the low annual precipitation ranging from 180 to 200 mm (Yang et al., 2015). The inner-year precipitation distribution is uneven as it accumulates predominantly during autumn (July–September), showing distinct wet and dry seasons. The main soil type of the flood plain is sandy loam, which allows a rapid and deep percolation. The aquifer thickness reaches a maximum of 30 m in the west edge of the area near the mountains, and is thinning towards the river plain with a depth of less than 1 m. On the other hand, the salinity increases from 0.5 g/L to 3 g/L as the aquifer thickness decreases.

Irrigation plays a key role in local hydrological processes during Spring irrigation (SI) and Winter irrigation (WI). Normally, SI spans the entire farming season (April to September) of three main crops (i.e., rice, wheat and corn) in this area. The average daily flow rate diverted from the Yellow River during SI is over 180 m^3/s with an annual peak daily flow rate above 300 m^3/s in mid-May when the water demands are overlapped for the three main crops. WI is necessary to freeze the topsoil in winter to preserve soil moisture and facilitate the plowing for the next farming season. The WI starts at the end of October and lasts until the end of November, with the daily average and annual peak flow rate around 200 m^3/s and 370 m^3/s, respectively. As a majority of farmland still adopt flood irrigation in the area, the irrigation return flow contributes to a substantial share of the streamflow. Typically, the local groundwater is not used for irrigation because it does not contain high nutrients in comparison with the water from the Yellow River. In addition, it has high salinity for most crops. Advanced irrigation technologies (e.g., pressurized wheel line sprinkler systems) are the only exception because these irrigation methods do not prefer sediment-rich water.

3. Data and methods

3.1. Dataset

MODIS provides one of the most widely used global LAI products in the research community (Xiao et al., 2017). The MODIS LAI time series product starts from 2000 (Myneni et al., 2002). Buermann et al. (2002) assessed the magnitude and interannual variations of field observed and RS-based LAI. Their results suggested that MODIS-derived LAI values its interannual variability showed reasonable agreement with ground measurements. In this study, The MODIS LAI product "MCD15A3H" Version 6 from 2007 to 2019 was used for the trend analysis. This LAI product is a 4-day composite data set with 500-m pixel size. According to the U.S. Geological Survey (Myneni, 2015), the algorithm chooses the best pixel available from all the acquisitions of both MODIS sensors located on NASA's Terra and Aqua satellites from within the 4-day period. Yan et al. (2016) also reported that "MCD15A3H" Version 6 is considerably better than the previous version. Version 6 can adequately capture the interannual variation of LAI and the general seasonality of all biomes, except for evergreen broadleaf forests, where poor quality retrievals are produced. Nevertheless, this shortcoming also exists in other satellite products, such as the CYCLOPES, GLASS, and the SPOT-VEGETATION system (Reygadas et al., 2019).

The MODIS LAI time series product is retrieved using the R software with the R package "MODISTools". Once the data were retrieved, the Land Data Operational Product Evaluation (LDOPE) tool was used to inspect the retrievals and remove those with poor quality. The obtained 4-day composite data set (with 0.5 km pixel size) was then aggregated into 4.5 km × 4.5 km tiles using the mean value to improve the robustness of results interpretation. Consequently, there are 200 tiles in the entire study area, as illustrated in Fig. 2. Finally, monthly LAI means were calculated on a tile-by-tile basis for each month from January 2007 to December 2019.

The time series datasets used in this study include daily streamflow time series from 13 drainage gauges, daily irrigation water flow time series from 6 canals, daily precipitation from 8 rain stations, daily mean temperature and evaporation from 2 climate stations, as well as daily groundwater head from 9 groundwater observation wells. These daily time series were all aggregated into monthly values from January 2007 to December 2019.

Future climate projections conducted by the regional climate model (RegCM) were used to infer future LAI changes. RegCM is based on the laws of physics, including the conservation of momentum, continuity equation, thermodynamic equation, and the hydrostatic equation, in the same way as GCMs do (Elguindi et al., 2013; Lu et al., 2019). Compared with global climate models (GCMs), RegCM is able to reflect regional details, such as the influences of local topography and land cover/use. Two grid points with a resolution of 50 km were used to represent the climate conditions for the two climate stations (Fig. 2). The gridded dataset (which spans from 2030 to 2099) was extracted from the RegCM simulations in Lu et al. (2019).

3.2. Monthly Mann-Kendal trend test

The monthly Mann Kendall (MK) trend test runs a separate MK trend test on each of *m* months separately. The MK trend test has been widely used for trend detection in hydrology and climatology (Zhang et al., 2001). In the test, the null hypothesis H_0 assumes that the sample is randomly ordered (i.e., no trend), while the alternative hypothesis H_1 of a two-sided test denotes that the sample follows a monotonic trend.

The Mann-Kendall test statistic $\boldsymbol{S}$ is calculated as:

$$S = \sum_{i=1}^{n-1} \sum_{j=i+1}^{n} sgn(x_j - x_i)$$

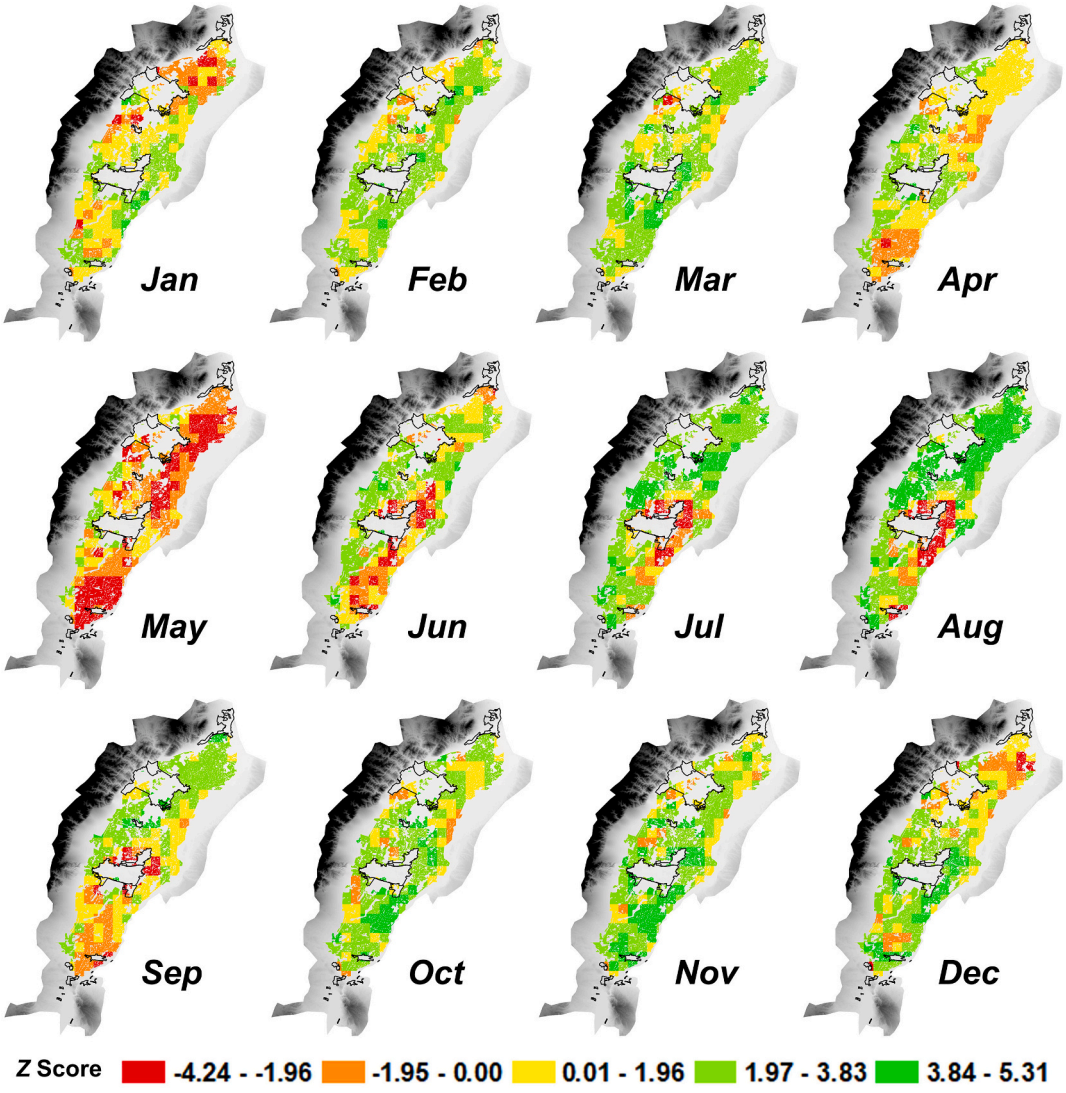

Fig. 3. ***Z*** scores of MK trend for monthly mean LAI value during 2007 to 2019.

$$sgn(x_j - x_i) = \begin{Bmatrix} if\,(x_j - x_i) < 0; then & -1 \\ if\,(x_j - x_i) = 0; then & 0 \\ if\,(x_j - x_i) > 0; then & 1 \end{Bmatrix}$$

where (x_1, …, x_n) denotes the total number of n samples for MK test (n should be greater than 10). The basic idea of MK test is that every sample point is compared to its preceding one in the time series, the positive values of S designate an increasing trend, while negative values of S represent a decreasing trend in the time series. For sample size $n > 10$, the test is accompanied using a normal distribution ($\sigma^2 = 1$) and mean ($\mu = 0$) with probability (E) and variance (Var) as shown below:

$$E(S) = 0$$

$$Var(S) = \frac{n(n-1)(2n+5) - \sum_p^q t_p(t_p - 1)(2t_p + 5)}{18}$$

where q is the tied groups representing observations having the same value, excluding the position of unique rank numbers, t_p is the number of data values in the p^{th} group and symbol (Σ) characterizes the summation of all the tied groups. However, if there are no tied groups in the data, this summary sequence may be ignored (Ashraf et al., 2021). Therefore, the standard MK test statistic Z for sample n is larger than ten is given by:

$$Z_{MK} = \begin{Bmatrix} \frac{S-1}{\sqrt{Var(S)}}, if\ \ S > 0 \\ 0, \quad\ \ if\ \ S = 0 \\ \frac{S+1}{\sqrt{Var(S)}}, if\ \ S < 0 \end{Bmatrix}$$

where Z_{MK} is used to check the null hypothesis, H_0. The value of Z_{MK} is compared with the normal distribution table of the two-tailed test at a confidence level of α. In a two-tailed test, the null hypothesis (H_0) is agreed for no-trend if the computed value of Z_{MK} fall between $-Z_{1-\alpha/2}$ and $Z_{1-\alpha/2}$. In this study, $\alpha = 0.05$ was used. At the 5% significance level, the null hypothesis of no trend is rejected if $|Z_{MK}| > 1.96$.

3.3. Stepwise clustered ensemble

Stepwise Clustered Ensemble (SCE) (Li et al., 2021) is used for identifying the relative significance of driving factors (e.g., temperature and precipitation) influencing the monthly LAI simulation. SCE is a tree-structured machine learning model that has been reported to outperform the well-known Random Forests (RF) (Breiman, 2001) in certain simulation tasks (Li et al., 2021). The SCE shares most advantages of RF for time series simulation owing to the (1) superior predictive accuracy with

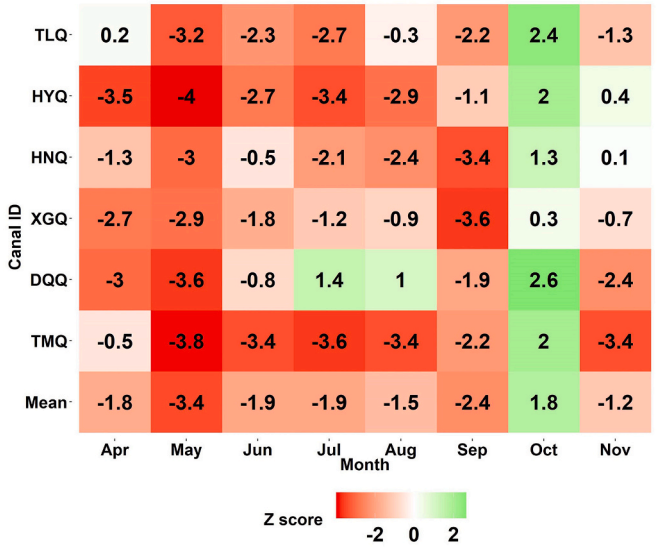

Fig. 4. ***Z*** scores of MK trend test for monthly mean irrigation (water diversion from the Yellow River) from 2007 to 2019. (For interpretation of the references to colour in this figure legend, the reader is referred to the web version of this article.)

little parameter tuning (Erdal and Karakurt, 2013; Fernández-Delgado et al., 2014; Li et al., 2019; Schmidt et al., 2020; Shortridge et al., 2016); (2) capacity to identify relevant predictor subsets in the presence of a large number of irrelevant predictors (Biau et al., 2008; Menze et al., 2011) and (3) the ability to produce interpretable inference process (Murdoch et al., 2019). Compared with other measures for identifying the relative significance, such as the mean decrease in impurity (MDI) used in RF and analysis of variance (ANOVA) in a linear regression model (Bénard, 2021; Lyu and Fan, 2021; Yang, 2020), the SCE can provide more reliable variable rankings due to the advanced tree-deduction process and the ability to deal with non-linearity (Li et al., 2021). More specifically, the Wilks feature importance (WFI) method embedded in SCE provides a less biased variable ranking than the mean decrease in impurity (MDI) and permutation feature importance (PFI) methods embedded in RF model, leading to a more faithful understanding of the related mechanisms (Li et al., 2021). In this study, the SCE will be applied to investigate the relative importance of contributing variables for the monthly LAI simulation.

Each SCA tree in an SCE grows in accordance with a random subset of predictors sampled without replacement and a bootstrapped version of the training set (same size to the original training set), drawn randomly from the initial training dataset with replacement. Such a bootstrap sampling process can leave about 1/3 of the training dataset as out-of-bag (OOB) data; these OOB data will not be involved in training the n^{th} SCA tree and thus can be used as a validation dataset for the corresponding tree. Since the validation result obtained from each SCA tree randomly covers 1/3 of the data over the training period, the ensemble (i.e., average) of these validation results from each tree of the forest can generally cover the entire data length over the training period when the number of tree is large.

4. Results analysis

4.1. Trend analysis of monthly LAI values

The MK trends based on the monthly mean LAI value have shown a significant spatial and temporal variability (Fig. 3). Specifically, significant increasing trends for vegetation growth are found for February and March in general, with ***Z*** scores between 0 and 1.96 (yellow tiles) and between 1.96 and 3.83 (light green tiles). Such increasing trends

Table 1
Water demands for three major crops.

Crop	Growing Stage	Start	End	Relative Water Requirement
Rice	Stage 1	9-May	9-Jun	25.6%
	Stage 2	10-Jun	29-Jun	9.5%
	Stage 3	30-Jun	29-Jul	28.6%
	Stage 4	30-Jul	8-Aug	13.2%
	Stage 5	9-Aug	28-Aug	16.0%
	Stage 6	29-Aug	3-Oct	7.1%
	All stages	9-May	3-Oct	100.0%
Wheat	Stage 1	6-Mar	4-Apr	7.2%
	Stage 2	30-Mar	20-Apr	4.9%
	Stage 3	18-Apr	11-May	15.6%
	Stage 4	10-May	30-May	25.5%
	Stage 5	27-May	26-Jun	34.6%
	Stage 6	20-Jun	7-Jul	12.1%
	All stages	6-Mar	7-Jul	100.0%
Corn	Stage 1	24-May	27-Jun	32.0%
	Stage 2	28-Jun	23-Jul	23.6%
	Stage 3	24-Jul	4-Sep	25.2%
	Stage 4	5-Sep	30-Sep	19.2%
	All stages	6-Mar	30-Sep	100.0%

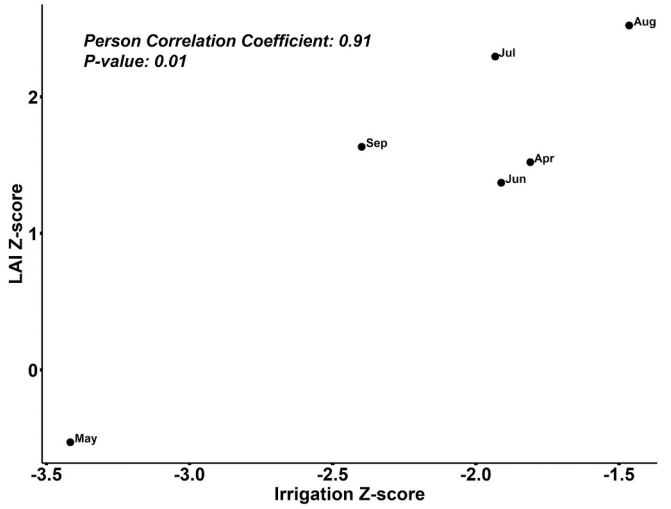

Fig. 5. Correlation between the ***Z*** scores of monthly water diversion and monthly LAI (regional mean) during the farming season. Note: the monthly LAI (based on the regional mean values) was calculated as the mean value of monthly LAI values over all the tiles.

gradually turn into decreasing trends and reach the overall lowest ***Z*** score in May, in which a majority of tiles are in orange (***Z*** scores between −1.95 to 0) and red (***Z*** scores between −1.96 to −4.24). After that, the decreasing trends gradually turn into increasing trends in June and reach the highest ***Z***score in August, with most of the tiles in the North area in deep green (***Z*** scores between 1.96 and 5.31). The exceptions are those tiles around the city of Yinchuan (as shown in Fig. 1), where the vegetation growth has experienced a significant decreasing trend during May to September (i.e., crop growing months). Most tiles have shown increasing trends in October and November, with scattered tiles showing a slightly decreasing trend. In December and January, some tiles in the North have indicated a decreasing trend.

The spatial patterns of the LAI trend are closely related to water resources management, agricultural development and urban expansion. From the perspective of water resources management, the irrigation system has been enforcing the "strictest water resources control regulations" (State Council of the People's Republic of China) since 2011, leading to a significant reduction of water diversion from the Yellow River. Fig. 4 shows the ***Z*** scores of MK trend test for monthly water diversions from 2007 to 2019. The most significant reduction of irrigation

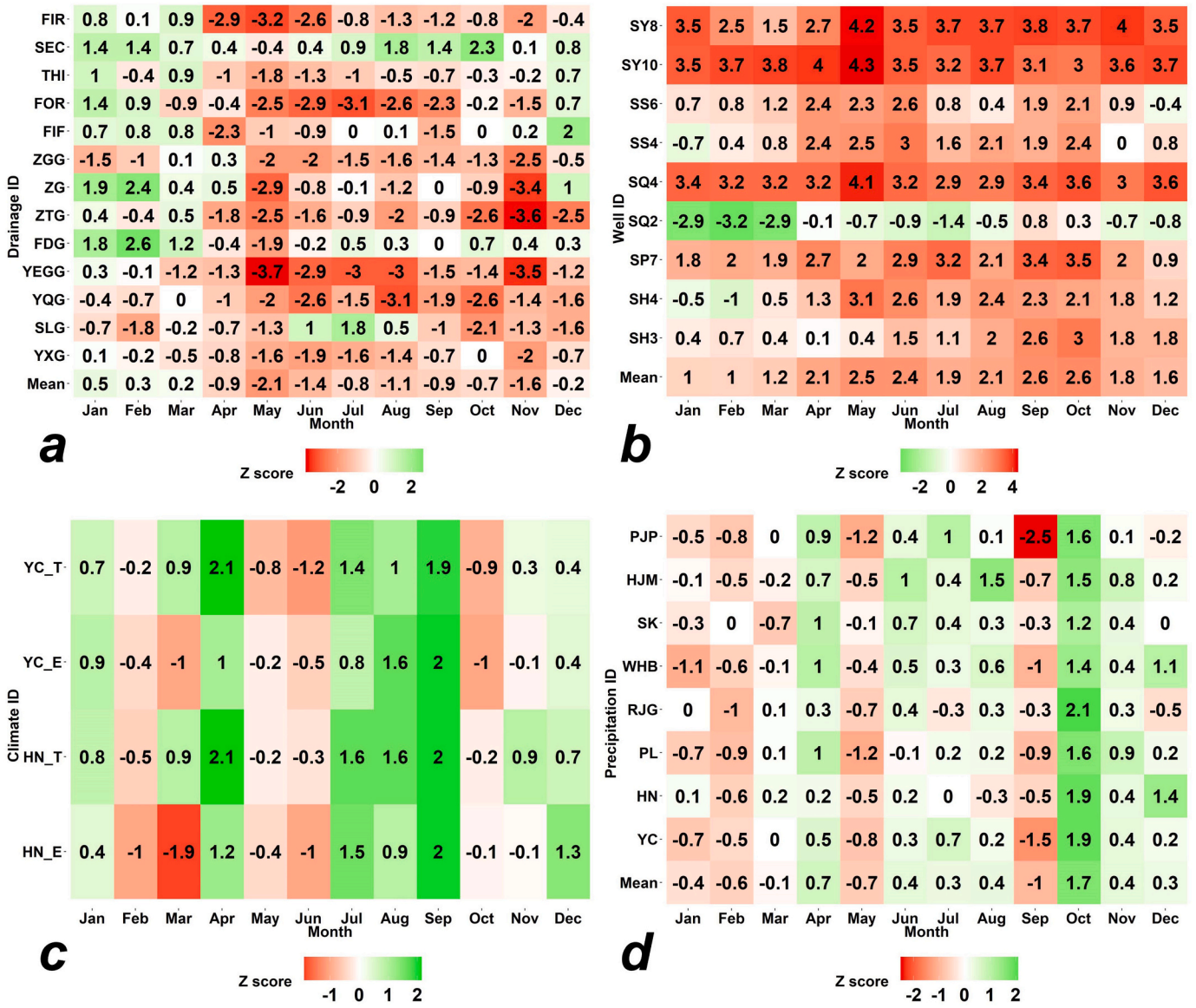

Fig. 6. Panels ***a*** to ***d*** show ***Z*** scores of MK trend test for monthly mean values of drainage discharge (upper left), groundwater depth (upper right), temperature and evaporation (bottom left), as well as precipitation (bottom right) during 2007 to 2019, respectively.

water happened in May, with the mean value of ***Z*** score equal to −3.4. Such a reduction explains why LAI experienced a significant decreasing trend in May. In fact, the crops in this area (i.e., rice, wheat and corn) require more water in their early growing stages than their later stages, as indicated in Table 1. This is verified by the positive correlation (Fig. 5) between the ***Z*** scores of monthly water diversion and monthly LAI (regional mean) during the farming season (i.e., April to September). In Fig. 5, vegetation growth in their later growing stages (i.e., July to September) is less impacted by the reduced irrigation than in their earlier stages (i.e., April to June). It is worth mentioning that even though the monthly irrigation water indicates decreasing trends, the monthly vegetation growth increased in general except May. Such increasing trends are mainly caused by the widespread water conservation practices, including water-saving irrigation technology, canal lining as well as conjunctive use of ground and surface water resources. Consequently, widespread water conservation practices have significantly improved irrigation water use efficiency (Mi et al., 2020) thus facilitating vegetation growth even with reduced irrigation water.

The decreasing trends of LAI during June to September are identified around the city of Yinchuan. According to Zhang et al. (2019), the city of Yinchuan has expanded from an area of 121.9 km^2 in 2006 to 175.6 km^2 in 2011, which then further expanded to 243.7 km^2 in 2017. The rapid expansion of the city inevitably occupied its surrounding farmlands, leading to the decreasing trend of LAI from June to September (i.e., the most vigorous period of crop growth). Meanwhile, the expansion of the city has led to increasing trends of LAI for October and November. This is because the urban greening can provide a high vegetation cover all year round, while the cropland will become bare ground after all the crops are harvested at the end of September. The widespread ecosystem restoration since 2003 is also responsible for the increasing trend of LAI for the non-farming months (i.e., October to March). According to Wang et al. (2018), the wetland area within the study area was increased from 431.7 km^2 in 2005 to 484.4 km^2 in 2016. Such widespread wetland restoration is evidenced by the increasing trend of water diversion in October (Fig. 4). These wetlands provide substantial water in the unsaturated zone to maintain the ecosystem health during the winter and early spring months (December to March). Fig. 6a shows that a majority of the drainages indicate an increasing trend of streamflow volumes from January to March, suggesting an increased soil water content.

The cropland in the North has been experiencing increasing trends of

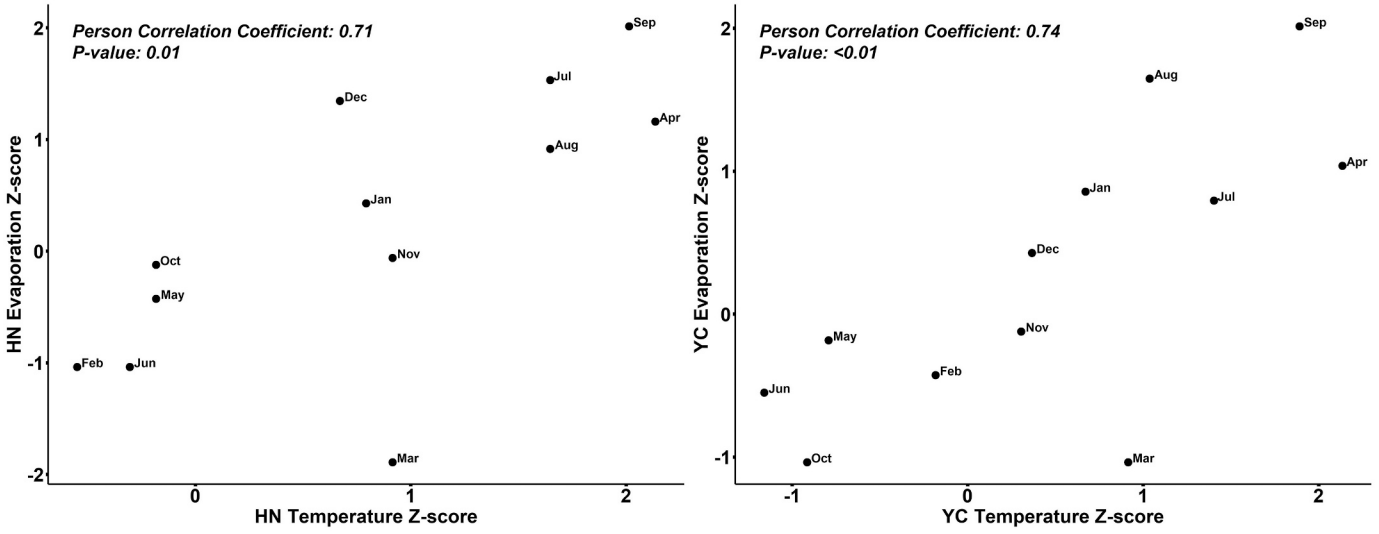

Fig. 7. Correlation between the ***Z*** scores of monthly temperature and evaporation.

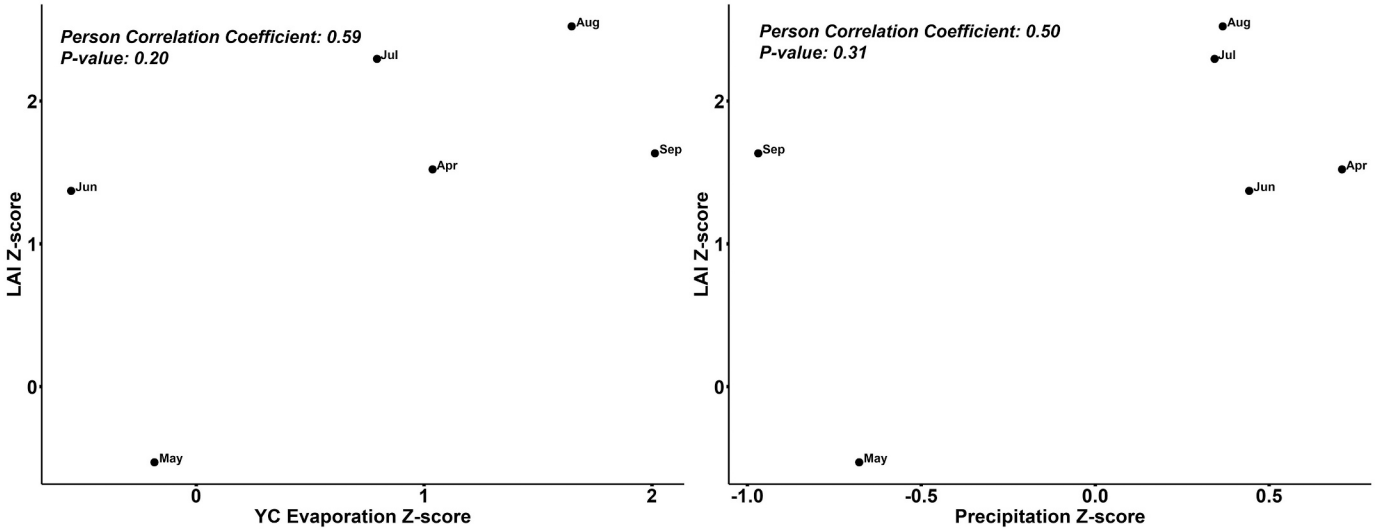

Fig. 8. The left panel shows a correlation between the ***Z*** scores of monthly evaporation and LAI; the right panel shows a correlation between the ***Z*** scores of monthly precipitation and LAI.

LAI from June to September (Fig. 3). Such increased vegetation growth mainly benefited from the exploitation of saline wasteland. Due to the extremely high evaporation and shallow groundwater table, around 33% of farmland suffered from high salinity with poor crop growth and low production (Wang and Li, 2009). Soil remediation for the saline wasteland has been a priority for local agricultural development. Since the last decade, several soil remediation practices, such as lowering the groundwater table and growing saline-alkali tolerant plants, have significantly improved the local soil conditions. The MK trends for groundwater table depth show that most of the observation wells indicate increasing trends with the highest ***Z*** score of 4.3 in May (Fig. 6b). The increased depth in the groundwater table has helped reduce the evaporation underground, thereby reducing the soil salinity and facilitating vegetation growth, leading to growing trends of LAI during the crop growing seasons(i.e., from June to September).

Fig. 6c and d show the MK trends for monthly mean temperature (T), evaporation (E) and precipitation of each weather stations. The correlations between the MK trends for temperature and evaporation are strongly correlated with Pearson correlation coefficients over 0.7 for Yinchuan (YC) and Huinong (HN) (Fig. 7). Even though the precipitation and evaporation positively contributed to the crop growth (Fig. 8), such correlation was less convincing (i.e., the ***p***-value for the correlation between LAI and precipitation equals 0.13; the ***p***-value for the correlation between LAI and evaporation in the city of Yinchuan equals 0.2). In fact, from January 2007 to December 2019, neither temperature nor precipitation indicated significant monthly trend (i.e., $|Z_{MK}|>1.96$; or at the 5% significance level). Therefore, there is no clear evidence that the climate variations from 2007 to 2019 contributed to the monthly trend of local vegetation growth.

4.2. Identifying relative importance of contributing variables through the monthly LAI simulation

Monthly LAI simulation was performed to investigate the relative importance of associated contributing factors, including monthly irrigation, evaporation, precipitation, and groundwater depth. The 1-month lagged impact of these factors was also considered in the simulation model. Therefore, the input-output structure for the monthly LAI simulation can be written as follows:

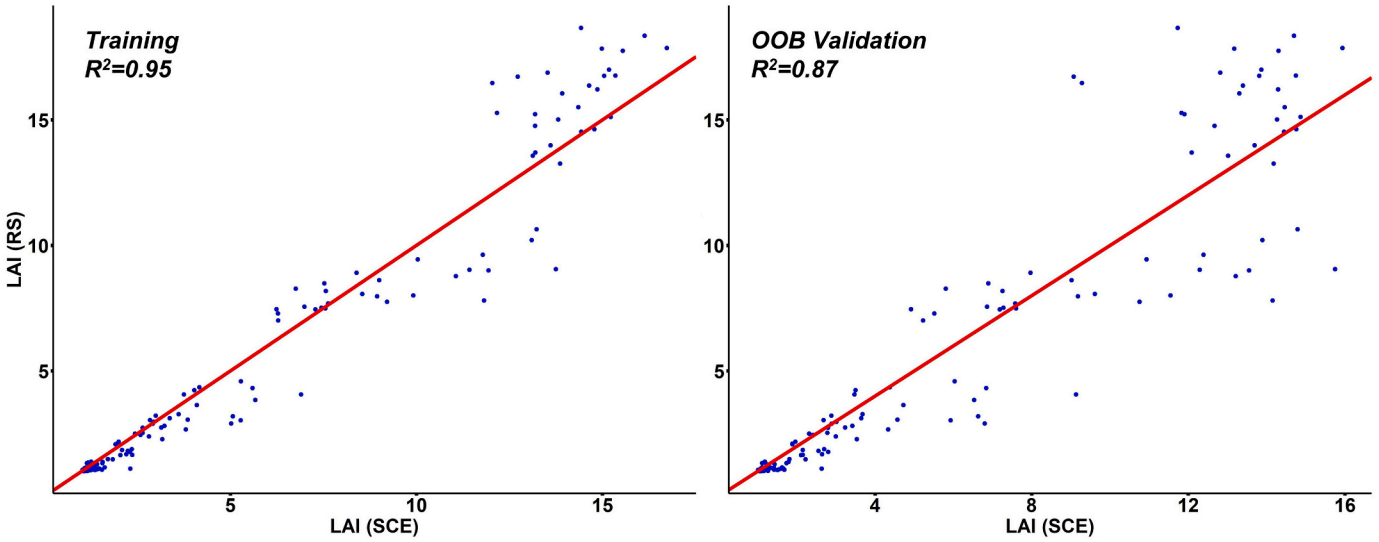

Fig. 9. SCE model simulations using training dataset (left) and out-of-bag (OOB) validation dataset (right). Note that the training and OOB validation period spans from January 2007 to December 2019; the red lines are 45-degree lines, which shows equality between the LAI measured on the vertical axis and the LAI measured on the horizontal axis. (For interpretation of the references to colour in this figure legend, the reader is referred to the web version of this article.)

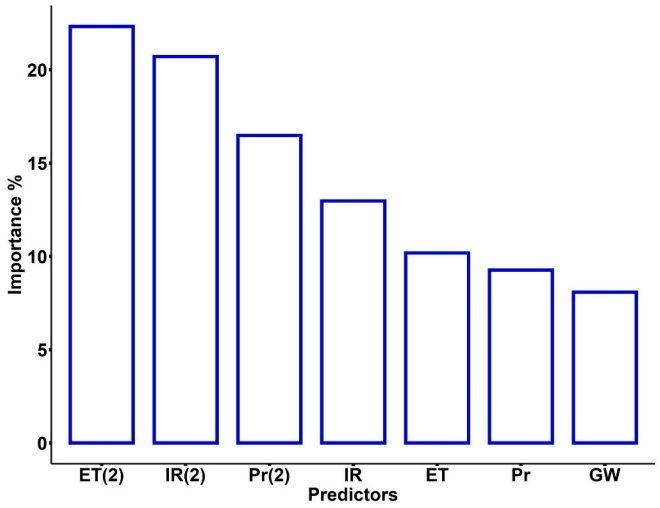

Fig. 10. Relative importance for contributing variables of LAI simulation. Note: **ET (2)** denotes 2-month (time step ***t*** and ***t-1***) averaged evaporation; the sum of relative importance equals one.

$$LAI_t = f(Pr_t, ET_t, IR_t, (Pr_t + Pr_{t-1})/2\,, (ET_t + ET_{t-1})/2\,, (IR_t + IR_{t-1})/2\,, GW_t) \quad (1)$$

where $\boldsymbol{LAI_t}$ represents the regional mean LAI value of month ***t***. ***Pr, ET, IR*** and ***GW*** represent monthly values of precipitation, evaporation, irrigation and groundwater level, respectively. ***f(x)*** represents the simulation functions of the SCE model.

Results indicate SCE model can well simulate monthly LAI value with the R^2 equals 0.87 based on the OOB validation dataset (Fig. 9). It should be noted that SCE underestimated some high LAI values and overestimated some mid-values. Two reasons are causing such discrepancy. The first is nonstationary of monthly LAI values. The SCE model, like most machine learning methods, takes observation (i.e., LAI values in this study) to be independent and identically distributed. This assumption is violated for time series data characterized by an increasing or decreasing trend, leading to distortions in simulation. The second reason is that SCE may fail to extrapolate beyond the range of the training dataset. For a particular SCA tree, if an LAI value in its OOB dataset falls outside the range of values in the training dataset, such an LAI value will likely to be overestimated or underestimated.

The analysis from WFI (Fig. 10) shows that 2-month averaged evaporation achieves the highest importance, followed by the 2-month averaged irrigation and precipitation. In addition, the monthly averaged predictors achieve lower importance scores than the 2-month averaged predictors. This result suggests that monthly vegetation growth response time to its driving forces is longer than one month. Such delayed response is also reported by Fang et al. (2019), who found the vegetation growth could respond to precipitation variations with the time lag ranging from 3 to 8 months in loess plateau. Notably, even though over 90% of agricultural water use in the study area is derived from the Yellow River (Ningxia Water Conservancy, 2007), the 2-month averaged precipitation still played a critical role in vegetation growth with the importance score equals 16.5%.

4.3. *Climate change may increase future crop water demands*

Analysis from WFI indicates that the importance of 2-month averaged irrigation ranked as the second-highest for monthly LAI simulation. Meanwhile, correlation analysis suggests that the significant change in irrigation (shown in Fig. 4) is the primary reason for the changing patterns of LAI with a *p*-value equal to 0.01 (shown in Fig. 5). These facts have led to a deduction that if monthly averaged evaporation or precipitation show significant trends in the future, the LAI patterns might experience substantial changes. To this end, the monthly trends of temperature and precipitation projections were examined based on the MK test. Fig. 11 shows that under the RCP 4.5 scenario, the annual precipitation and temperature for Yinchuan area do not have a significant trend annually. While, under the RCP 8.5 scenario, a slightly increasing trend can be found for annual mean precipitation, and a significant increasing trend can be found for annual mean temperature.

In order to better present the gradual change of the future climate, the future period is separated into three time slices: early-mid twenty-first century (2030–2050), mid-late twenty-first century (2051–2070), and late-twenty-first century (2070–2099). Future projections suggest that an increase of only 36 mm precipitations is expected in the Yinchuan area from early-mid to the late-twenty-first century under the RCP 8.5 scenario. Moreover, an increase of 1 °C in daily mean temperature is expected from early-mid to the mid-late twenty-first century under the RCP 8.5 scenario, while such an increase will reach 2.3 °C

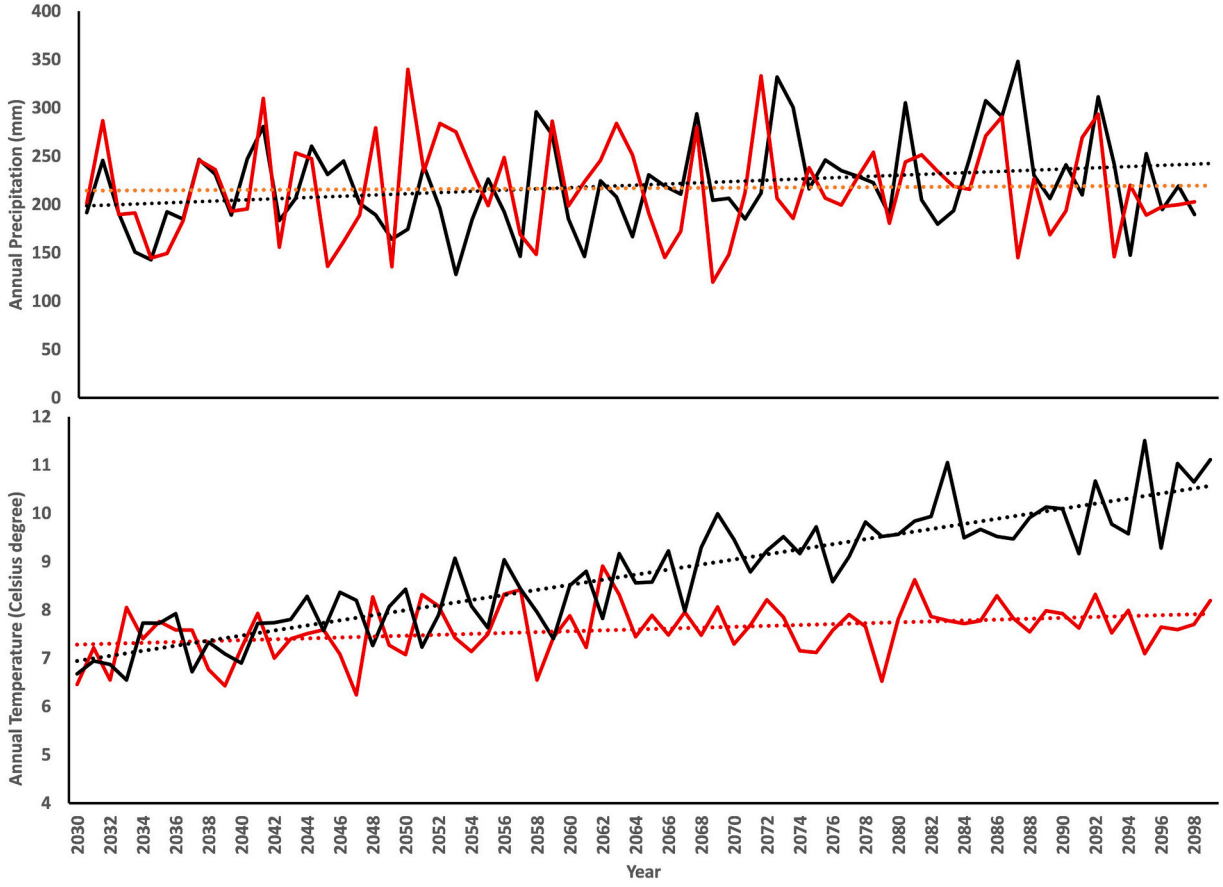

Fig. 11. Projections for annual precipitation and temperature for Yinchuan region (50 km × 50 km area centered at the latitude of 38.416 and longitude of 106.185) under the RCP 4.5 (red) and 8.5 (black) scenarios. (For interpretation of the references to colour in this figure legend, the reader is referred to the web version of this article.)

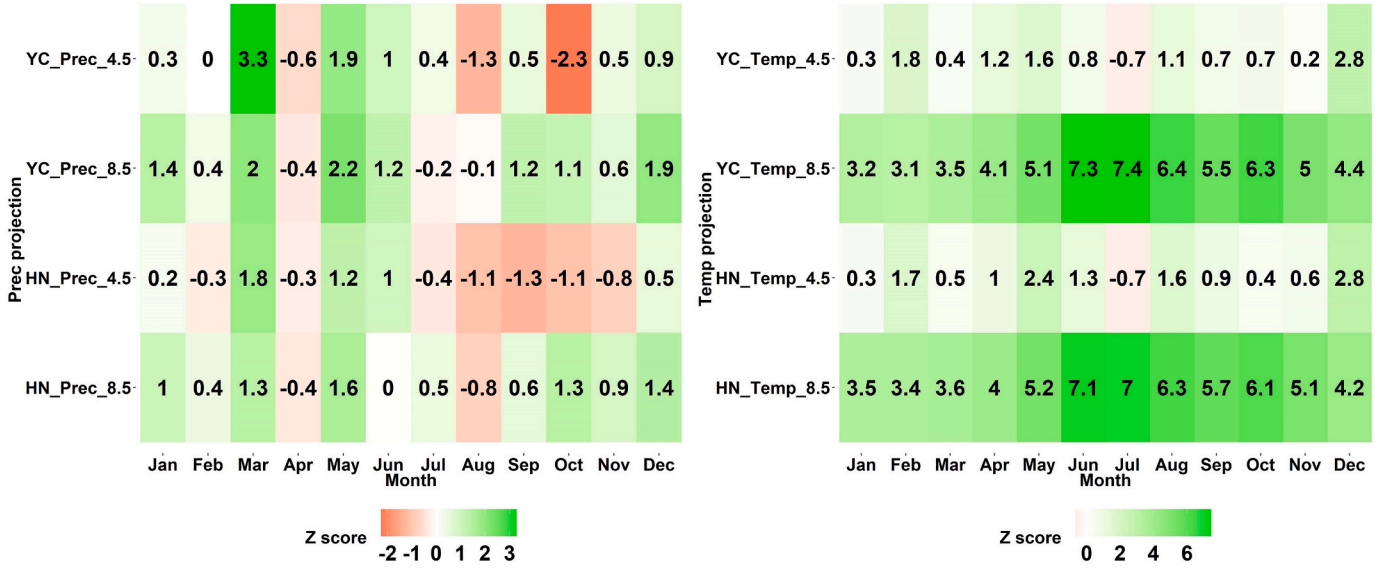

Fig. 12. *Z* scores of the MK trend test for projected monthly mean values of precipitation (left) and temperature (right) from January 2030 to December 2099. Note: YC_Prec_4.5 and YC_Prec_8.5 indicate the projected precipitation for the Yinchuan area (50 km × 50 km area centered at the latitude of 38.416 and longitude of 106.185) based on RCP 4.5 and 8.5 scenarios, respectively. RegCM grid for the Huinong area is centered at the latitude of 39.3195 and longitude of 106.839.

from early-mid to late twenty-first century.

The MK trend analysis for monthly mean precipitation projections suggests that no significant trends for precipitation (i.e., $|Z_{MK}|<1.96$) can be identified for most of the months under either RCP 4.5 or 8.5 scenarios (Fig. 12). The exceptional months include an increasing trend in March and a decreasing trend in October under RCP 4.5 scenario in

the Yinchuan area, as well as an increasing trend in March and May under RCP 8.5 scenario in the Yinchuan area. These increases in precipitation will positively contribute to crop growth in early spring. However, such an increase in precipitation may not alleviate the water shortage in the Yinchuan area because the evaporation may increase even higher under the RCP 8.5 scenario. The MK trend analysis for monthly mean temperature projections suggests that there might be a slightly increasing trend under the RCP 4.5 scenario and a significant increasing trend under the RCP 8.5 scenario. In particular, a warmer December is expected with a significant increasing trend (Z equals 2.8 for both Yinchuan and Huinong area) under the RCP 4.5 scenario. The warmer winter will lead to reduced ground-frozen time, which will challenge the irrigation practice since the soil moisture will deplete quicker in winter, affecting the crop growth of next year. Such a situation will worsen under the RCP 8.5 scenario, in which the highest increase in temperature would happen in June and July, followed by August, October and September. As a consequence, the summer will last much longer than the present. The long-lasting summer will inevitably increase the evaporation in the crop growing months, thereby increasing the agricultural water demand.

5. Remarks and conclusions

In this study, MK trend analysis was performed to investigate the spatial and temporal change of LAI on a monthly basis. Compared with previous trend analysis studies focused on a yearly or seasonal basis, such a study at a finer temporal resolution provided more valuable and detailed information supporting agriculture management. Combined with the trend analysis of several contributing variables influencing LAI, irrigation was considered a critical factor leading to the nonstationary LAI. Water conservation practices, city expansion, soil remediation practices and wetland restoration were also responsible for the spatial and temporal change of LAI. There was no clear evidence that climate variations during the study period influenced LAI. The analysis from WFI indecated that the response time of monthly vegetation growth to its driving forces is longer than one month. The 2-month average evaporation achieved the highest importance, followed by the 2-month average irrigation and precipitation. According to future climate projections, no significant trend for precipitation can be identified for most of the months under either RCP 4.5 or 8.5 scenarios. At the same time, significant increasing trends for air temperature were identified for every month under the RCP 8.5 scenario, especially for the crop growing months.

The main contribution of this paper is to demonstrate the MK trend analysis for LAI on a monthly basis can provide more valuable information than on a yearly and seasonal basis. In irrigated watersheds, such trend analysis may help to diagnose monthly crop growth conditions and their reasoning. Decision-makers can then optimize irrigation scheduling month to month for dealing with crop water deficit. In this study, the crop growth in May experienced significant degradation, and such degradation may worsen in the future due to the increased evaporation in winter. More importantly, irrigators may face dryer and longer summers in the future, which inevitably challenge the agriculture industry of Ningxia.

In this study, only one regional climate model was used to investigate future climate change. In the future, an ensemble of regional climate models should be preferred to improve the robustness of the result. In addition, an improved interpretable machine learning model should be proposed in the future to consider the nonstationary effect of LAI simulation. Such simulation models may answer the question of how much irrigation water will be required under climate change.

Author statement

Kailong Li: Conceptualization; Data curation; Formal analysis; Investigation; Methodology; Software; Writing - original draft; Validation. **Guohe Huang**: Supervision; Funding acquisition. **Xiaoyue Zhang**: Writing - Reviewing and Editing; **Chen Lu**: Data curation – climate data; **Shuo Wang**: Writing - Reviewing and Editing.

Declaration of competing interest

The authors declare that they have no conflict of interest.

Acknowledgements

This research was supported by Canada Research Chair Program, Natural Science and Engineering Research Council of Canada, Western Economic Diversification (15269), and MITACS. We are also very grateful for the helpful inputs from the Editor and anonymous reviewers.

References

Alton, P.B., 2018. Decadal trends in photosynthetic capacity and leaf area index inferred from satellite remote sensing for global vegetation types. Agric. For. Meteorol. 250, 361–375.
Ashraf, M.S., et al., 2021. Streamflow variations in monthly, seasonal, annual and extreme values using Mann-Kendall, Spearmen's rho and innovative trend analysis. Water Resour. Manag. 35 (1), 243–261.
Bénard, C., et al., 2021. Interpretable random forests via rule extraction. International Conference on Artificial Intelligence and Statistics (PMLR), 937–945.
Biau, G., Devroye, L., Lugosi, G., 2008. Consistency of random forests and other averaging classifiers. J. Mach. Learn. Res. 9 (Sep), 2015–2033.
Breda, N.J., 2003. Ground-based measurements of leaf area index: a review of methods, instruments and current controversies. J. Exp. Bot. 54 (392), 2403–2417.
Breiman, L., 2001. Random Forests. Machine Learning 45 (1), 5–32.
Buermann, W., et al., 2002. Analysis of a multiyear global vegetation leaf area index data set. J. Geophys. Res. Atmos. 107 (D22) (ACL 14–1-ACL 14–16).
Chen, J.M., Cihlar, J., 1996. Retrieving leaf area index of boreal conifer forests using Landsat TM images. Remote Sens. Environ. 55 (2), 153–162.
Cortés, J., et al., 2021. Where are global vegetation greening and browning trends significant? Geophys. Res. Lett. 48 (6) (e2020GL091496).
Elguindi, N., et al., 2013. Regional climate model RegCM user manual version 4.4. In: The Abdus Salam International Centre for Theoretical Physics, Strada Costiera, Trieste, Italy October, 21, p. 54, 2013.
Erdal, H.I., Karakurt, O., 2013. Advancing monthly streamflow prediction accuracy of CART models using ensemble learning paradigms. J. Hydrol. 477, 119–128.
Fang, W., et al., 2019. Probabilistic assessment of remote sensing-based terrestrial vegetation vulnerability to drought stress of the loess plateau in China. Remote Sens. Environ. 232, 111290.
Fernández-Delgado, M., Cernadas, E., Barro, S., Amorim, D., 2014. Do we need hundreds of classifiers to solve real world classification problems? J. Mach. Learn. Res. 15 (1), 3133–3181.
Gregory, R., Funge-Smith, S., Baumgartner, L., 2018. An Ecosystem Approach to Promote the Integration and Coexistence of Fisheries within Irrigation Systems.
23rd ICID International Congress on Irrigation and Drainage. (Accessed 15 Sep 2020).
Jiang, B., Liang, S., Wang, J., Xiao, Z., 2010. Modeling MODIS LAI time series using three statistical methods. Remote Sens. Environ. 114 (7), 1432–1444.
Jiang, C., et al., 2017. Inconsistencies of interannual variability and trends in long-term satellite leaf area index products. Glob. Chang. Biol. 23 (10), 4133–4146.
Karimi, S., et al., 2020. Estimation of Forest Leaf Area Index Using Meteorological Data: Assessment of Heuristic Models. J. Environ. Inform. 36 (2).
Kendall, M.G., 1948. Rank Correlation Methods. Charles Griffin and Company, London.
Li, J., Wang, Z., Lai, C., Zhang, Z., 2019. Tree-ring-width based streamflow reconstruction based on the random forest algorithm for the source region of the Yangtze River, China. Catena 183, 104216.
Li, K., Huang, G., Baetz, B., 2021. Development of a Wilks feature importance method with improved variable rankings for supporting hydrological inference and modelling. Hydrology and Earth System Sciences 25, 4947–4966.
Liang, S., Yi, Q., Liu, J., 2015. Vegetation dynamics and responses to recent climate change in Xinjiang using leaf area index as an indicator. Ecol. Indic. 58, 64–76.
Liu, X., Lian, Y., Ke, S., 2009. Analysis on water demand for ecosystem protection in Yellow River Delta. J. Hydraul. Eng. 40 (8), 956–965.
Lu, C., 2019. Long history and future benefits of ancient irrigation system in Ningxia. J. China Flood Drought Manag. 29 (5), 60–62 (in Chinese).
Lu, C., Huang, G., Wang, X., 2019. Projected changes in temperature, precipitation, and their extremes over China through the RegCM. Clim. Dyn. 53 (9), 5859–5880.
Lyu, X.D., Fan, Y.R., 2021. Characterizing Impact Factors on the Performance of Data Assimilation for Hydroclimatic Predictions through Multilevel Factorial Analysis. J. Environ. Inform. 38 (1), 68–82.
Mann, H.B., 1945. Nonparametric tests against trend. Econometrica 245–259. https://doi.org/10.2307/1907187.
Menze, B.H., Kelm, B.M., Splitthoff, D.N., Koethe, U., Hamprecht, F.A., 2011. On oblique random forests, Joint European Conference on Machine Learning and Knowledge Discovery in Databases. Springer, pp. 453–469.

Mi, L., et al., 2020. Evolution of groundwater in Yinchuan oasis at the upper reaches of the Yellow River after water-saving transformation and its driving factors. Int. J. Environ. Res. Public Health 17 (4), 1304.
Monteith, J., Unsworth, M., 2013. Principles of Environmental Physics: Plants, Animals, and the Atmosphere. Academic Press.
Mu, C., et al., 2000. Wetland ecosystems formation and its protection in Yellow River Delta. The journal of applied ecology 11 (1), 123–126.
Murdoch, W.J., Singh, C., Kumbier, K., Abbasi-Asl, R., Yu, B., 2019. Definitions, methods, and applications in interpretable machine learning. Proc. Natl. Acad. Sci. 116 (44), 22071–22080. https://doi.org/10.1073/pnas.1900654116.
Myneni, R.B., et al., 2002. Global products of vegetation leaf area and fraction absorbed PAR from year one of MODIS data. Remote Sens. Environ. 83 (1–2), 214–231.
Myneni, R., et al., 2015. MCD15A3H MODIS/Terra+Aqua Leaf Area Index/FPAR 4-day L4 Global 500m SIN Grid V006 [Data set]. NASA EOSDIS Land Processes DAAC. https://doi.org/10.5067/MODIS/MCD15A3H.006. Accessed 2021-10-26.
Ningxia Water Conservancy, 2007-2019. Ningxia Water Resources Bulletin 2007–2019. Ningxia Water Conservancy, Ningxia, China.
Raheem, N., et al., 2015. A framework for assessing ecosystem services in Acequia irrigation communities of the upper Río Grande watershed. Wiley Interdiscip. Rev. Water 2 (5), 559–575.
Rasul, A., Ibrahim, S.a., Onojeghuo, A.R., Balzter, H., 2020. A trend analysis of leaf area index and land surface temperature and their relationship from global to local scale. Land 9 (10), 388.
Reygadas, Y., Jensen, J.L., Moisen, G.G., 2019. Forest degradation assessment based on trend analysis of MODIS-leaf area index: a case study in Mexico. Remote Sens. 11 (21), 2503.
Schmidt, L., Heße, F., Attinger, S., Kumar, R., 2020. Challenges in applying machine learning models for hydrological inference: a case study for flooding events across Germany. Water Resour. Res. 56 (5) https://doi.org/10.1029/2019WR025924 e2019WR025924.
Shortridge, J.E., Guikema, S.D., Zaitchik, B.F., 2016. Machine learning methods for empirical streamflow simulation: a comparison of model accuracy, interpretability, and uncertainty in seasonal watersheds. Hydrol. Earth Syst. Sci. 20 (7) https://doi.org/10.5194/hess-20-2611-2016.
Shrestha, N., Wang, J., 2020. Water Quality Management of a Cold Climate Region Watershed in Changing Climate. J. Environ. Inform. 35 (1).
Opinions of the State Council on Applying the Strictest Water Resources Control System. (Accessed 15 Sep 2020).
Wang, H., Li, J., 2009. Discussions on remediation of soil in saline wasteland for the ancient Yellow River irrigation system [in Chinese]. Sci. Technol. Inform. 04 (2009), 2.
Wang, H., Yang, Z., Saito, Y., Liu, J.P., Sun, X., 2006. Interannual and seasonal variation of the Huanghe (Yellow River) water discharge over the past 50 years: connections to impacts from ENSO events and dams. Glob. Planet. Chang. 50 (3), 212–225.
Wang, Y., Zhao, X., Li, Y., Wang, Y., Z T., 2018. Influence of dynamic evolution of wetland area on local climate effect in Ningxia plain [in Chinese]. Ecol. Environ. Sci. 27 (7), 1251–1259.
Xiao, Z., Liang, S., Jiang, B., 2017. Evaluation of four long time-series global leaf area index products. Agric. For. Meteorol. 246, 218–230.
Yan, K., et al., 2016. Evaluation of MODIS LAI/FPAR product collection 6. Part 2: validation and intercomparison. Remote Sens. 8 (6), 460.
Yang, J., et al., 2015. Drought adaptation in the Ningxia Hui autonomous region, China: actions, planning, pathways and barriers. Sustainability 7 (11), 15029–15056. https://doi.org/10.3390/su71115029.
Yang, Z., 2020. DCT-Based Least-Squares Predictive Model for Hourly AQI Fluctuation Forecasting. J. Environ. Inform. 36 (1).
Yin, Y., et al., 2017. Nonlinear variations of forest leaf area index over China during 1982–2010 based on EEMD method. Int. J. Biometeorol. 61 (6), 977–988.
Zhang, Z., Deng, S., 1987. The development of irrigation in China. Water Int. 12 (1–2), 46–52.
Zhang, X., Harvey, K.D., Hogg, W., Yuzyk, T.R., 2001. Trends in Canadian streamflow. Water Resour. Res. 37 (4), 987–998.
Zhang, J., Bai, L., Yang, M., 2019. Spatial and temporal evolution of Yinchuan urban expansion in the last 30 years [in Chinese]. Res. Soil Water Conserv. 05, 359–365.
Yuan, Z., et al., 2021. EVI Indicated Spatial-Temporal Variations in Vegetation and Their Responses to Climatic and Anthropogenic Factors in the Chinese Mainland Since 2000s. J. Environ. Inform. In press.
Zhang, W., et al., 2021. Temporal and spatial variations in the leaf area index and its response to topography in the Three-River source region, China from 2000 to 2017. ISPRS Int. J. Geo Inf. 10 (1), 33.
Zhu, Z., et al., 2017. Attribution of seasonal leaf area index trends in the northern latitudes with “optimally” integrated ecosystem models. Glob. Chang. Biol. 23 (11), 4798–4813.